Appropriate Boundary Conditions for a Pressure Driven Boundary Layer

P.J. Richards[1] and S.E. Norris[1]

[1]Department of Mechanical Engineering
University of Auckland, Auckland 1142, New Zealand

Abstract

Velocity and turbulence property profiles are derived for an equilibrium pressure driven atmospheric boundary layer for CFD models using the *k-ε, k-ω and SST* turbulence model. By comparison with the Deaves and Harris model it is shown that such a pressure driven boundary layer is a reasonable model for the lower half of the atmospheric boundary layer where the shear stress decreases approximately linearly with height. The profiles derived satisfy equilibrium of the momentum and both turbulence property conservation equations. It is shown that using these profiles as the inlet conditions on an empty domain results in outlet profiles which are almost identical to the inlet values. It is also shown that using profiles intended for a shear driven situation, but without the driving shear stress, leads to significant changes as the flow relaxes towards matching the free slip boundary condition at the top of the domain.

1. Introduction

At the first Computational Wind Engineering Conference Richards and Hoxey (1993) recommended modelling the atmospheric surface layer as a horizontally-homogeneous turbulent surface layer (HHTSL), which is one with constant properties in directions tangential to the ground and hence the only variation is along the vertical axis. Since the pressure is constant the flow is driven by a shear stress at the upper surface of the layer, and this is constant throughout the layer, equalling the shear stress at the wall. As noted by Panofsky and Dutton (1984) the surface layer is the lowest part of the atmospheric boundary layer (ABL), where the shear stress is almost constant and which in moderate to strong winds may extend 100m or more above the ground. Velocity and turbulence property profiles, together with the associated boundary conditions, were proposed for CFD studies using the standard *k-ε* turbulence model (Launder and Spalding, (1974)) and were shown to satisfy horizontal homogeneity provided the various constants satisfied a particular relationship. Richards and Hoxey (1993) concluded "In order to adequately model the atmospheric surface layer the boundary conditions, turbulence model and associated constants must be consistent with each other". In this regard the boundary conditions included the inlet velocity and turbulence property profiles, the wall functions used at the ground, the driving shear stress and the diffusion of turbulence properties at the top of the domain.

Richards and Hoxey (1993) has been cited numerous times and while many of these citations are from authors who have simply utilised the recommendations, a number contain related discussions. Bottema (1997) has discussed the difference between the level of turbulence kinetic energy (TKE) observed in the atmospheric surface layer and those given by the standard constants of many turbulence models. Blocken et al. (2007) focus on wall function problems and the relationship between the wind engineering roughness length and the sand grain roughness commonly used in internal flows. Hargreaves and Wright (2007) discuss some of the difficulties with implementing the Richards and Hoxey (1993) boundary conditions and note that many computational wind engineers adopt only a subset of these and as a result the turbulence profiles decay along the fetch. They also noted the over production of turbulence kinetic energy in cells near the ground. Richards and Norris (2011) have revisited the analysis of the constant shear stress surface layer and have extended the analysis to include a number of common turbulence models. In addition they have provided an explanation of the excessive production of turbulence kinetic energy often observed in the near wall region.

The Richards and Hoxey (1993) recommendations have found their way into various guidelines including those for predicting the pedestrian wind environment by COST (European Cooperation in the field of Scientific and Technical Research) Action C14 "Impact of Wind and Storms on City Life and Built Environment", Working group 2 – CFD Techniques, as reported by Franke (2006), and the Architectural Institute of Japan (Tominaga et al. (2008)).

2. Horizontally Homogeneous Turbulent Surface Layer

Richards and Hoxey (1993) modelled a HHTSL by proposing velocity and turbulence property profiles, together with the associated boundary conditions, for the standard *k-ε* turbulence model and showed that these satisfied horizontal homogeneity provided certain additional conditions were satisfied. Richards and Norris (2011) use an alternative approach to derive the profiles directly from the conservation and equilibrium equations for a HHTSL

associated with a particular turbulence model. For example with the standard k-ε model and a rough wall with U=0 at the roughness height z=z_0, these yield:

$$U = \frac{u_\tau}{\kappa_{k\varepsilon}} \ln\left(\frac{z}{z_0}\right) \tag{1}$$

$$k = \frac{u_\tau^2}{\sqrt{C_\mu}} \tag{2}$$

$$\varepsilon = \frac{u_\tau^3}{\kappa_{k\varepsilon} z} \tag{3}$$

where u_τ is the friction velocity associated with the wall shear stress, which within the surface layer equals the shear stress at all levels

$$\tau = \tau_w = \rho u_\tau^2 \tag{4}$$

where ρ is the air density.

The derivation showed that the turbulence model effectively chooses its own value for von Kármán's constant κ, such that the usual k-ε turbulence model constants $C_{\varepsilon 1}$ = 1.44, $C_{\varepsilon 2}$ = 1.92, C_μ = 0.09 and σ_ε = 1.3 give

$$\kappa_{k\varepsilon} = \sqrt{\left(C_{\varepsilon 2} - C_{\varepsilon 1}\right)\ \sigma_\varepsilon \sqrt{C_\mu}} = 0.4237 \tag{5}$$

which is slightly larger than the commonly accepted value κ = 0.4, which will be used in the remainder of this paper.

The form of Eqs. (1-3) only differs from those given by Richards and Hoxey (1993) in terms of the definition of the height at which the velocity is zero. To implement such profiles the shear stress is imposed at the upper boundary of the domain, a zero flux condition is set for k, and the flux of ε across the top boundary is prescribed as,

$$\frac{\mu_t}{\sigma_\varepsilon}\frac{d\varepsilon}{dz} = -\frac{\rho u_\tau^4}{\sigma_\varepsilon z} \tag{6}$$

Hargreaves and Wright (2007) note that in their experience "many computational wind engineers adopt only a subset of the Richards and Hoxey boundary conditions (i.e. those at the inlet) and assume that the boundary layer will be maintained up to the point at which the building is located". However they show that this is not the case, even in the absence of obstructions, and that the velocity and turbulence profiles decay along the fetch under these conditions. In their numerical modelling they initially investigate an empty domain, deliberately ignore the shear stress at the top of the domain, "since many practitioners ignore this requirement", but instead decide "that a symmetry condition would suffice" for the demonstration. Without the driving shear stress the problem becomes a pressure driven boundary layer, within which the shear stress varies with height, and while equilibrium profiles may exist these will be different from the constant shear stress case. The turbulence kinetic energy development from a computation similar to that undertaken by Hargreaves and Wright (2007) is shown in Fig. 1, where the turbulence kinetic energy is seen to gradually develop from the Richards and Hoxey (1993) uniform value, which is appropriate for a shear driven boundary layer, towards values appropriate for a pressure driven boundary layer. The uniform turbulence kinetic energy value derived by Richards and Hoxey (1993) is a consequence of the constant shear stress, which is an approximation to reality. Noting this limitation Yang et al. (2009) have proposed alternative k and ε turbulence property profiles and in their discussion they state: "The new inflow turbulence boundary conditions for the standard k–ε model that have been presented in this paper are different from those proposed by Richards and Hoxey (1993). In particular, the new profile for k shows a decay of k with height, while the profile for k by Richards and Hoxey (1993) is constant with height. Note that the decrease with height is typically observed in measurements." However these profiles have been derived by assuming a log-law velocity profile and splitting the turbulence kinetic energy conservation equation into two independent parts, production equal to dissipation and zero diffusion, and solving these. The profiles derived in this manner do not generally satisfy either the dissipation or momentum equations and hence, while they may not change rapidly, are not in equilibrium. The derivation of appropriate boundary conditions for an alternative approximation, that of a pressure driven boundary layer, by using the full set of conservation equations is the subject of this paper.

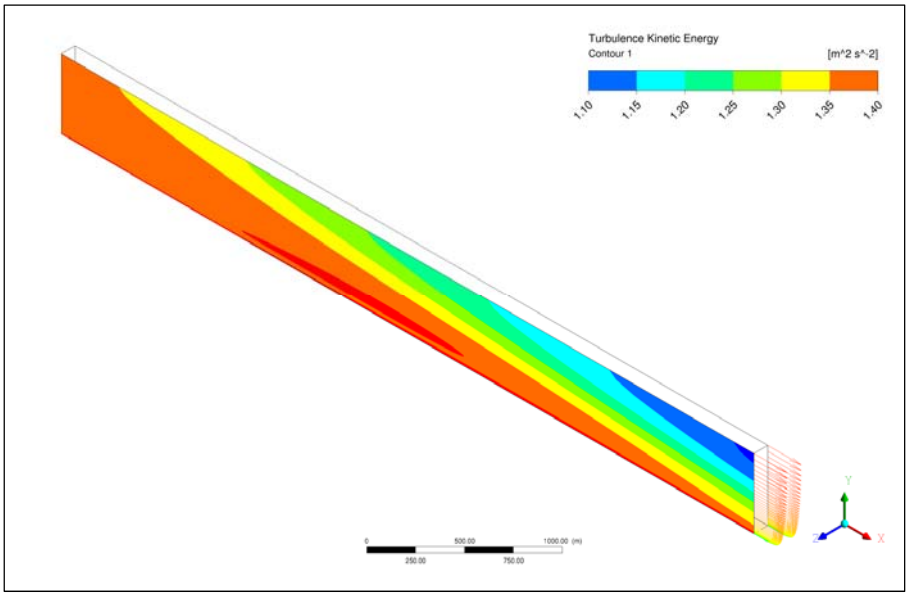

Fig. 1. Development of the turbulence kinetic energy in a pressure driven boundary layer with inlet conditions appropriate for a shear driven boundary layer.

3. The Deaves and Harris Model of the Atmospheric Boundary Layer

Deaves and Harris (1978) provided a mathematical model of the characteristics of the ABL in strong winds. This model has been adopted as the basis for wind speed and turbulence characteristics of the ABL in various wind loading codes including AS/NZS 1170.2 (2011). The primary equations for this model are:

The gradient height (h) is

$$h = \frac{u_\tau}{6f} \tag{7}$$

where the Coriolis parameter

$$f = 2\Omega \sin\phi \tag{8}$$

with Ω the rate of rotation of the earth (72.9×10^{-6} rad/s) and ϕ the latitude. In this paper the latitude used as an example is 45°, a mid-latitude that in the northern hemisphere passes through the USA, Canada and numerous countries in Europe and Asia and in the southern hemisphere through New Zealand, Argentina and Chile. As a result $f = 1.03 \times 10^{-4}$ rad/s.

The velocity profile is

$$U(z) = \frac{u_\tau}{\kappa}\left(\ln\left(\frac{z}{z_0}\right) + 5.75\left(\frac{z}{h}\right) - 1.875\left(\frac{z}{h}\right)^2 - 1.333\left(\frac{z}{h}\right)^3 + 0.25\left(\frac{z}{h}\right)^4 \right) \tag{9}$$

which, since 1+5.75-2×1.875-3×1.333+4×0.25=0, has zero gradient at $z = h$.

Eqs. (7-9) can be used to determine the gradient height, gradient wind speed and friction velocity given the surface roughness and a reference velocity at a known height. For example Hargreaves and Wright (2007) used a test case where the surface roughness length z_0=0.01 m and the reference velocity at z=6 m was set to U(6 m)=10 m/s, which yields a gradient height h=1005 m, gradient wind speed $U(h)$= 22.25 m/s and a friction velocity u_τ= *0.622* m/s. This test case will also be used in this paper but with the gradient height rounded to 1000m.

The equilibrium of forces in the atmosphere is a balance between pressure gradients, shear stresses, centripetal acceleration and Coriolis effects. Deaves and Harris (1978) concluded that the shear stress (τ) gradient was most appropriately modelled as a quadratic decay of the form

$$\tau(z) = \rho u_\tau^2 \eta^2 \tag{10}$$

where $\eta = 1 - z/h$, which is a dimensionless fraction of the gradient height measured from the top downwards.

In addition they suggest the standard deviation of the along-wind component of the wind velocity is given by

$$\frac{\sigma_u(z)}{u_\tau} = 2.63\eta\left[0.538 + 0.09\ln(z/z_0)\right]^m \tag{11}$$

where the exponent $m=\eta^{16}$.

ESDU 85020 (1985) supplements the Deaves and Harris (1978) equations by providing formulas for the ratio of the transverse and vertical standard deviations to the along-wind standard deviation as follows:

$$\frac{\sigma_v(z)}{\sigma_u(z)} = 1 - 0.22\cos^4\left(\frac{\pi}{2}\frac{z}{h}\right) \tag{12}$$

$$\frac{\sigma_w(z)}{\sigma_u(z)} = 1 - 0.45\cos^4\left(\frac{\pi}{2}\frac{z}{h}\right) \tag{13}$$

From Eqs. (11-13) the variation of the transverse and vertical standard deviations with height can be determined. Hence noting that the turbulence kinetic energy

$$k = \frac{\sigma_u^2 + \sigma_v^2 + \sigma_w^2}{2} \tag{14}$$

$$\frac{k}{u_\tau^2} = \frac{\sigma_u^2}{2u_\tau^2}\left(1 + \left(\frac{\sigma_v}{\sigma_u}\right)^2 + \left(\frac{\sigma_w}{\sigma_u}\right)^2\right) \tag{15}$$

Fig. 2(a) shows the variation of the shear stress, as given by Eq. (10) (labelled "$\tau/\rho u_\tau^2$ Quad"), and the standard deviation ratios with height and Fig. 2(b) the variation of the three standard deviations and the turbulence kinetic energy. These profiles suggest that the shear stress is never constant and that while $k \approx 8u_\tau^2$ for a small range of heights $0.005 < z/h < 0.05$, the general behaviour is a decay similar to that of the shear stress. It may also be noted that the low height k values are much larger than the $k = 3.33u_\tau^2$ given by Eq. (2). Richards and Hoxey (1993) recognised this apparent anomaly, which has been further discussed by Bottema (1997) and Richards and Norris (2011) amongst others. The primary explanation is related to the much higher levels of inactive low frequency turbulence which is present in the atmospheric boundary layer in comparison with the smaller scale turbulent boundary layers used to set the standard turbulence model constants. This low frequency turbulence contributes significant energy while having very little effect on the Reynolds stresses and hence may be considered inactive. In many ways these low frequency fluctuations may be more appropriately considered to be a slowly varying mean flow rather than part of the turbulence. Richards et al. (2007) showed that during boundary layer wind tunnel testing of the Silsoe cube, where with relatively low linear scale ratio the low frequency turbulence cannot exist in the confined space, the mean pressure coefficients could be matched even though the turbulence intensity was much lower provided the high frequency end of the spectrum was matched. In that wind tunnel test measurements showed $k = 3.18u_\tau^2$ at building height. Hence in CFD modelling the values of k used might be considered to represent high-pass filtered full-scale turbulence. But even this filtered turbulence will decrease with height.

As noted in ESDU 85020 (1985) in the lower atmosphere the Reynolds shear stress can be approximated by the linear function

$$\tau(z) = \rho u_\tau^2(1 - 2z/h) \tag{16}$$

which is also depicted in Fig. 2(a), labelled "$\tau/\rho u_\tau^2$ Linear".

While it is possible to construct computational models that include pressure gradients, Coriolis effects and the shear stresses, this is probably overly complex for many practical problems. Fortunately, as will be shown in the following section, an equilibrium pressure driven boundary layer will have a Reynolds shear stress that varies linearly with height in a manner similar to Eq. (16). The associated velocity and turbulence property profiles will be derived.

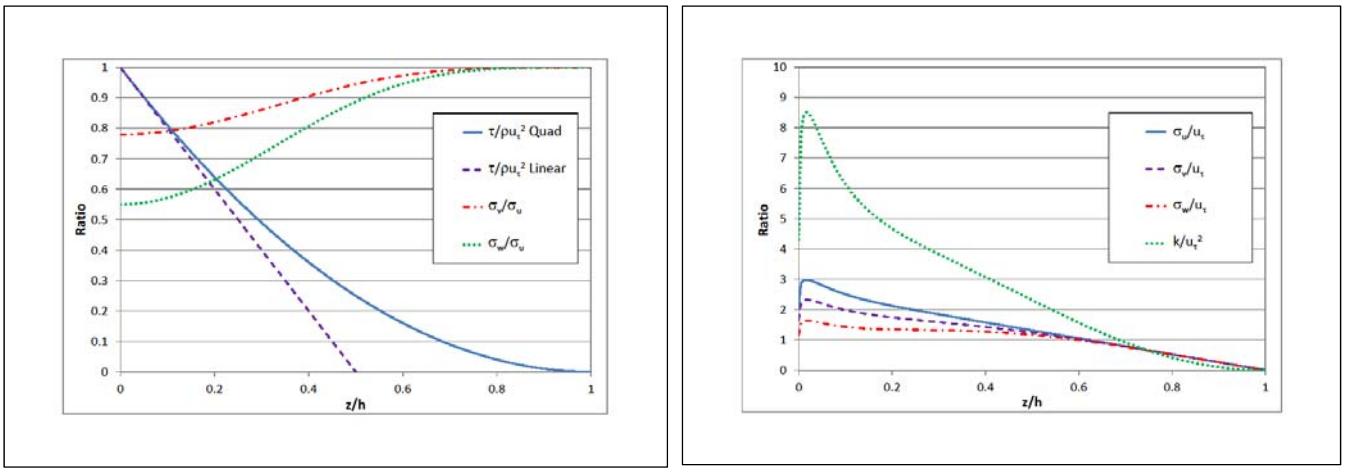

Fig. 2. (a) Shear stress and standard deviation ratio profiles and (b) the variation of standard deviations and TKE with height in the atmospheric boundary layer.

4. Semi-Analytic Analysis of the Equilibrium Pressure Driven Boundary Layer

As noted in section 2, many computational wind engineers will set up a problem by choosing a turbulence model, defining the inlet conditions and will probably define the roughness of the ground plane. However they will leave the top boundary as a default free-slip symmetry boundary. As a result the flow is driven through the domain by a pressure difference between inlet and outlet. In this section we seek to find velocity and turbulence property profiles that will result in an equilibrium boundary layer under such conditions. The turbulence models considered are the standard k-ε model of Launder and Spalding (1974); the Wilcox (1993) k-ω model and the blending of these in the SST model of Menter (1994), although a similar analysis is possible with most of the standard turbulence models. The solution domain considered, see Fig. 3, is an empty domain of height H but arbitrary width and length. The pressure is assumed to decrease at a steady rate in the streamwise direction, while being constant across all heights. All other variables are assumed to be independent of both the x and y co-ordinates but may vary with height z above the ground plane.

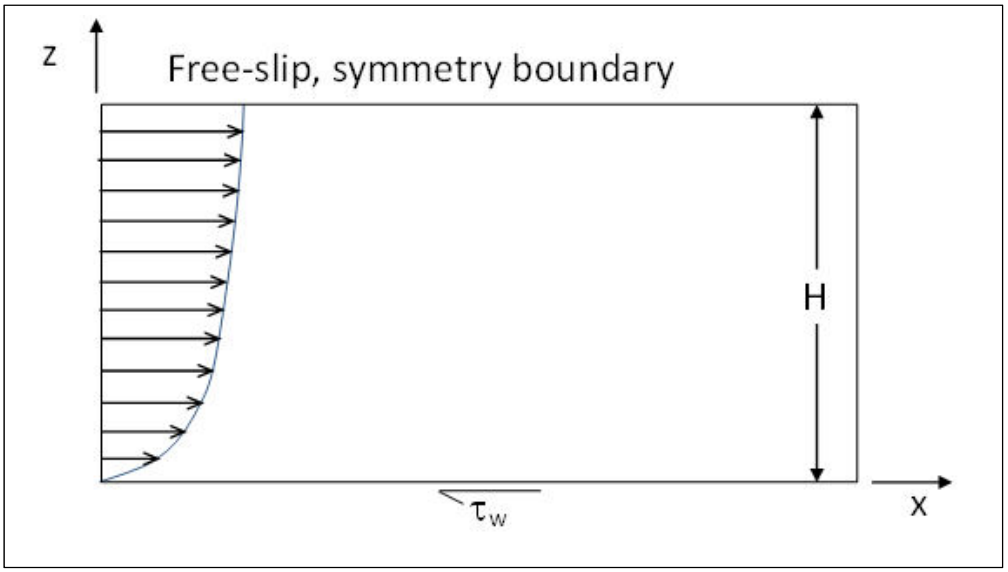

Fig. 3. Layout schematic of the solution domain.

In many CFD problems the inlet conditions are defined in terms of the velocity and turbulence property profiles. The computer code is then used to determine such things as the wall shear stress or the pressure differential required to drive the prescribed flow through the domain. In this analysis the order is reversed and it is assumed that the driving pressure gradient is known and the analysis seeks to determine the velocities and turbulence profiles which would match this driving force. While these conditions can be obtained by running a CFD model with either a long fetch or with cyclic boundary conditions, the initial approach taken here is to analyse the basic equations and then to compare the results with CFD.

If the flow is in equilibrium then the forces must be balanced both on the entire domain and on a sub-domain up to height z. As a result for the complete domain

$$\frac{dp}{dx}LHW = \tau_w LW = \rho u_\tau^2 LW \quad \text{or} \quad \frac{dp}{dx}H = \tau_w = \rho u_\tau^2 \tag{17}$$

where τ_w is the shear stress at the wall (ground), W the width and L the length of the domain. From the balance of forces on the sub-domain we obtain

$$\frac{dp}{dx}LzW + \tau(z)LW = \tau_w LW \text{, which together with Eq. (17) yields } \tau(z) = \tau_w(1 - z/H) \tag{18}$$

Eqs. (17) and (18) apply to any equilibrium pressure driven boundary layer of depth H, irrespective of the turbulence model used. If H=h/2, that is half the gradient height as given by Eq. (7), then Eq. (18) is equivalent to Eq. (16). If the domain depth is less than half the gradient height, equilibrium profiles can still be derived but the shear stress gradient will be greater than that in the lower part of the ABL.

In a rough wall, high Reynolds number boundary layer such as the ABL, the turbulent shear stress is much larger than the viscous shear stress right down to the level of the roughness. Hence in this analysis it is assumed that

$$-\rho\overline{u'w'} >> \mu\frac{dU}{dz} \tag{19}$$

In addition it is assumed that the Boussinesq eddy viscosity approximation, which is part of most two equation turbulence models, applies such that

$$-\rho\overline{u'w'} = \mu_t\frac{dU}{dz} \tag{20}$$

where the calculation of the eddy viscosity μ_t will depend on the particular turbulence model. Note that in a log law atmospheric boundary layer with u_τ= *0.622* m/s and z_0=0.01m then even at z=0.01m, $\mu_t = \rho\kappa u_\tau z = 3\times10^{-3}$ Pas, about 170 times larger than the laminar viscosity and it increases almost linearly with height. As a result within the equilibrium pressure driven boundary layer considered here

$$\tau(z) = \mu_t\frac{dU}{dz} \tag{21}$$

To go beyond this point requires the choice of a particular turbulence models. While the analysis has been carried out with both the standard k-ε and Wilcox k-ω models, only the former will be described in detail since the analysis is very similar. The approach taken involves analytic development of the equations as far as possible and only resorts to a numerical approach in the final stage, it is hence referred to hereafter as the "Semi-Analytic" (SA) method. Due to the complex nature of the blending of these two models in the SST model no attempt has been made to use the semi-analytic approach on that model, although CFD solutions are presented in Section 5.

With the standard k-ε model the eddy viscosity is related to the turbulence kinetic energy (k) and its rate of dissipation (ε) by

$$\mu_t = C_\mu\rho\frac{k^2}{\varepsilon} \tag{22}$$

Since the solution sought is for the equilibrium situation the total derivatives of the turbulence properties is zero and so the standard conservation equations are simplified to

$$\rho\frac{Dk}{Dt} = 0 = \mu_t\left(\frac{dU}{dz}\right)^2 - \rho\varepsilon + \frac{d}{dz}\left(\frac{\mu_t}{\sigma_k}\frac{dk}{dz}\right) \tag{23}$$

$$\rho\frac{D\varepsilon}{Dt} = 0 = C_{\varepsilon1}\mu_t\left(\frac{dU}{dz}\right)^2\frac{\varepsilon}{k} - C_{\varepsilon2}\rho\frac{\varepsilon^2}{k} + \frac{d}{dz}\left(\frac{\mu_t}{\sigma_\varepsilon}\frac{d\varepsilon}{dz}\right) \tag{24}$$

where the model constants are as given in Section 2 in association with Eq. (5), plus σ_k = 1.0.

The velocity derivative in Eqs. (23) and (24) can be replaced by using the relationships in Eqs. (18) and (21) yielding

$$0 = \mu_t \left(\frac{\tau_w (1 - z/H)}{\mu_t} \right)^2 - \rho\varepsilon + \frac{d}{dz}\left(\frac{\mu_t}{\sigma_k} \frac{dk}{dz} \right) \tag{25}$$

$$0 = C_{\varepsilon 1}\mu_t \left(\frac{\tau_w (1 - z/H)}{\mu_t} \right)^2 \frac{\varepsilon}{k} - C_{\varepsilon 2}\rho \frac{\varepsilon^2}{k} + \frac{d}{dz}\left(\frac{\mu_t}{\sigma_\varepsilon} \frac{d\varepsilon}{dz} \right) \tag{26}$$

In order to obtain a more general result these equations can be transformed into a non-dimensional form by normalising the variables in the following manner

$$z^* = \frac{z}{H}, \quad U^* = \frac{U}{u_\tau}, \quad k^* = \frac{k}{u_\tau^2}, \quad \varepsilon^* = \frac{\varepsilon H}{u_\tau^3}, \quad \mu_t^* = \frac{\mu_t}{\rho u_\tau H}, \quad \tau^* = \frac{\tau}{\rho u_\tau^2} \tag{27}$$

and eliminating the eddy viscosity by using Eq. (22), which gives

$$0 = \frac{(1 - z^*)^2}{C_\mu} \frac{\varepsilon^*}{k^{*2}} - \varepsilon^* + \frac{d}{dz^*}\left(\frac{C_\mu k^{*2}}{\sigma_k \varepsilon^*} \frac{dk^*}{dz^*} \right) \tag{28}$$

$$0 = C_{\varepsilon 1} \frac{(1 - z^*)^2}{C_\mu} \frac{\varepsilon^{*2}}{k^{*3}} - C_{\varepsilon 2} \frac{\varepsilon^{*2}}{k^*} + \frac{d}{dz^*}\left(\frac{C_\mu k^{*2}}{\sigma_\varepsilon \varepsilon^*} \frac{d\varepsilon^*}{dz^*} \right) \tag{29}$$

This pair of linked equations has been solved using finite-difference approximations. The boundary conditions used are given in Table 1 and the resulting profiles plotted in Fig. 4. At the top of the domain both k^* and ε^* reach their minimum, but both are still finite since the diffusion (last terms in Eqs. (28-29)) is matched by the dissipation (2nd to last terms).

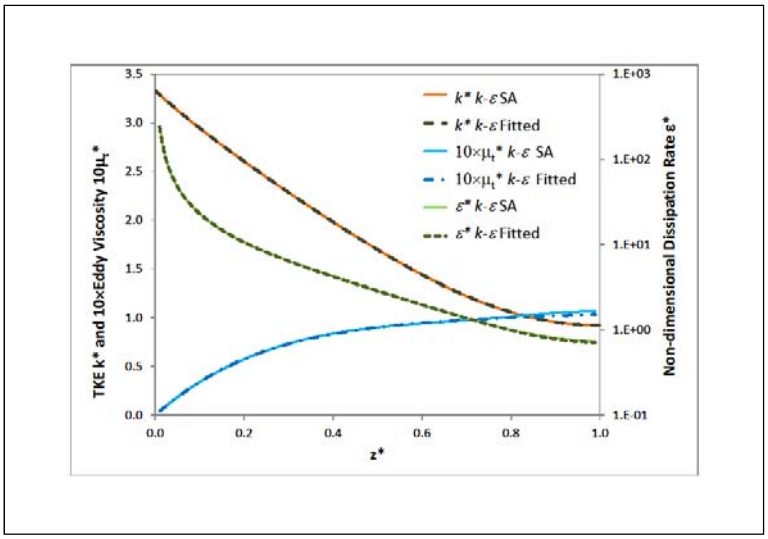

Fig. 4. Calculated and fitted equilibrium turbulence property profiles for the k-ε turbulence model. For clarity the eddy viscosity has been multiplied by 10 and ε^* is plotted against a log scale secondary axis. The solid lines are the computed values while the dashed lines are the fitted relationships given by Eqs. (31, 34 & 37).

Table 1. Boundary conditions for the turbulence property equations.

Variable	Near ground, $z^* \to 0$	Top, $z^* = 1$
k^*	$k^* \to \frac{1}{\sqrt{C_\mu}}$	$\frac{dk^*}{dz^*} = 0$
ε^*	$\varepsilon^* = \frac{C_\mu^{0.75} k^{*1.5}}{\kappa z^*}$	$\frac{d\varepsilon^*}{dz^*} = 0$

In order to make the results more readily accessible polynomial expressions have been fitted to the computed values. The form chosen for the non-dimensional TKE was

$$k^* = f(z^*) = k_1 + k_2(1-z^*)^2 + k_3(1-z^*)^4 + k_4(1-z^*)^6 \tag{30}$$

since this fitted the data well and had zero gradient at $z^*=1$, that is $z=H$. The semi-analytic k^* values are matched to within ±0.3% by

$$k^* = f(z^*) = 0.921 + 3.533(1-z^*)^2 - 1.926(1-z^*)^4 + 0.801(1-z^*)^6 \tag{31}$$

It may be noted that at $z^* = 0$, $k^* = 3.33$, as required by the boundary conditions. In later equations $f(z^*)$ is used to represent this polynomial.

It was found that the dissipation rate could not be readily matched by a similar polynomial and that while the eddy viscosity could be matched, a simpler result could be obtained by first calculating the velocity gradient from

$$\frac{dU^*}{dz^*} = \frac{\tau^*}{\mu_\tau^*} = \frac{1-z^*}{\mu_\tau^*} \tag{32}$$

The functional form chosen for the velocity derivative is given by

$$\frac{dU(z)}{dz} = \frac{u_\tau}{\kappa H}\left(\frac{H}{z} + U_1 + 2U_2\left(\frac{z}{H}\right) + 3U_3\left(\frac{z}{H}\right)^2 + 4U_4\left(\frac{z}{H}\right)^3\right) \tag{33}$$

The velocity gradient in non-dimensional form is therefore

$$\frac{dU^*}{dz^*} = g(z^*) = \frac{1}{\kappa}\left(\frac{1}{z^*} + U_1 + 2U_2 z^* + 3U_3 z^{*2} + 4U_4 z^{*3}\right) \tag{34}$$

Determining the coefficients in this function has been conducted by calculating the product of the non-dimensional height and the velocity gradient and then fitting a fourth order polynomial. Due to numerical instabilities at small z^* von Karman's constant κ could not be accurately determined and so was prescribed as 0.4. In addition the final constant U_4 was marginally adjusted to ensure the gradient was zero at $z^*=1.0$. Fig. 5 shows the finite difference derived data and the fitted curve.

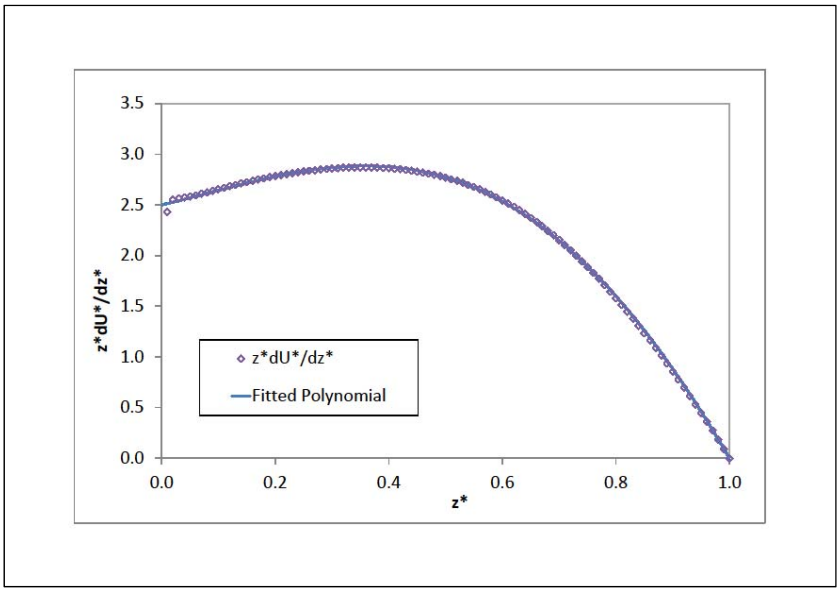

Fig. 5. Velocity gradient data from the finite difference solution and the polynomial curve fitted to it.

For this turbulence model the semi-analytic data is well matched by

$$z^* \frac{dU^*}{dz^*} = 2.5 + 1.32z^* + 1.926z^{*2} - 8.172z^{*3} + 2.426z^{*4} \tag{35}$$

From which the velocity gradient expression is

$$\frac{dU^*}{dz^*} = g(z^*) = \frac{1}{0.4}\left(\frac{1}{z^*} + 0.528 + 2\times 0.385 z^* - 3\times 1.090 z^{*2} + 4\times 0.243 z^{*3}\right) \tag{36}$$

where the constants have been rearranged to match Eq. (35) and the results entered into Table 2. An expression for the eddy viscosity may be obtained by substituting the polynomial $g(z^*)$, as defined by Eq. (36), into a rearranged Eq. (21):

$$\mu_\tau^* = \frac{1 - z^*}{g(z^*)} \tag{37}$$

and hence the dissipation rate from Eq. (22) giving

$$\varepsilon^* = \frac{C_\mu f^2(z^*) g(z^*)}{1 - z^*} \tag{38}$$

The resulting fits are shown in Fig. 4. The agreement is not as good as for TKE but the fitted relationships match to within ±4% and these errors are greatest near the top of the boundary layer.

Eq. (34) may be integrated to give the velocity profile

$$U^* = \frac{1}{\kappa}\left(\ln(z^*) + U_1 z^* + U_2 z^{*2} + U_3 z^{*3} + U_4 z^{*4}\right) + \text{constant} \tag{39}$$

The integration constant is evaluated by using an appropriate velocity boundary condition at the ground. If the simple condition of a rough wall with U=0 at $z=z_0$ and $z_0 << H$ is used then the constant can be taken as $-\ln(z_0^*)/\kappa$. Hence Eq. (39) becomes

$$U^* = \frac{1}{\kappa}\left(\ln\left(\frac{z^*}{z_0^*}\right) + U_1 z^* + U_2 z^{*2} + U_3 z^{*3} + U_4 z^{*4}\right) \tag{40}$$

This can be transformed back into a dimensional form as

$$U(z) = \frac{u_\tau}{\kappa}\left(\ln\left(\frac{z}{z_0}\right) + U_1\left(\frac{z}{H}\right) + U_2\left(\frac{z}{H}\right)^2 + U_3\left(\frac{z}{H}\right)^3 + U_4\left(\frac{z}{H}\right)^4\right) \tag{41}$$

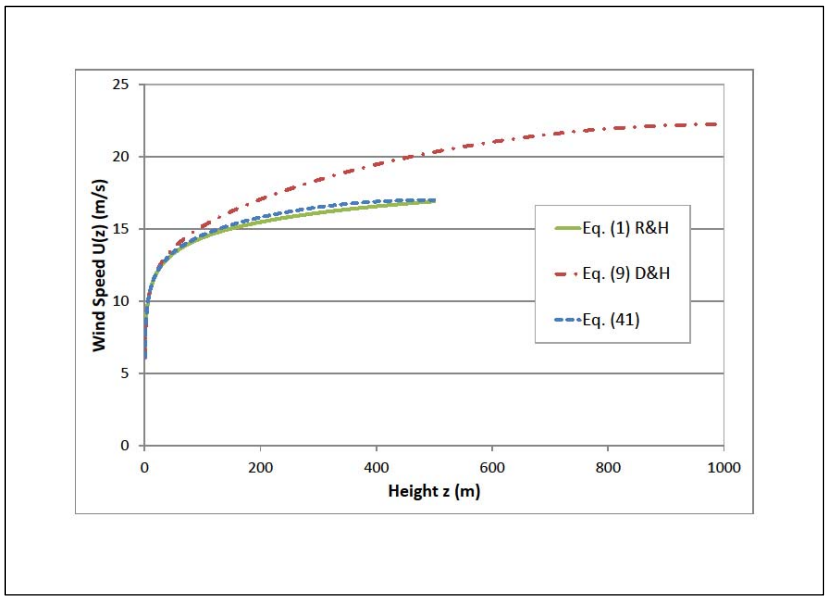

Fig. 6. A comparison of velocity profiles given by Eqs. (1, 9 and 41) for the Hargreaves and Wright (2007) test case.

This is similar in form to the Deaves and Harris (1978) model, however the coefficients are quite different. Fig. 6 shows a comparison between the simple log law used by Richards and Hoxey (1993) as given in Eq. (1), the Deaves and Harris (1978) model from Eq. (9) and Eq. (41), for the Hargreaves and Wright (2007) test case

mentioned in Section 3. All three curves are very similar at low heights, where they essentially reduce to the logarithmic term, however they diverge at heights above about 30 m. The simple log law never reaches a zero gradient due to the constant shear stress assumption, whereas the current model flattens off at half the gradient height, while the Deaves and Harris equation continues to increase up to the full gradient height.

The corresponding dimensional forms for the turbulence properties are

$$k(z) = u_\tau^2 \left(k_1 + k_2 \left(1 - \frac{z}{H}\right)^2 + k_3 \left(1 - \frac{z}{H}\right)^4 + k_4 \left(1 - \frac{z}{H}\right)^6 \right) \tag{42}$$

$$\begin{aligned} \varepsilon(z) &= \frac{C_\mu k(z)^2}{\kappa u_\tau z} \left(\frac{1 + U_1(z/H) + 2 \times U_2(z/H)^2 + 3 \times U_3(z/H)^3 + 4 \times U_4(z/H)^4}{1 - z/H} \right) \\ &= \frac{C_\mu k(z)^2}{\kappa u_\tau z} \left(1 + (1 + U_1)(z/H) + (1 + U_1 + 2U_2)(z/H)^2 + (1 + U_1 + 2U_2 + 3U_3)(z/H)^3 \right) \end{aligned} \tag{43}$$

The simplification in Eq. (43) is possible because the polynomial in the numerator has zero value at $z=H$ and hence has 1-z/H as a factor. Fig. 7 contrasts the turbulence property profiles for a pressure driven boundary layer as determined from Eqs. (31) and (38), or from CFD calculation, with those for the shear driven boundary layer analysed by Richards and Hoxey (1993) as given in Eqs. (2) and (3). It is clear that the decreasing shear stress with height has a dramatic effect on the turbulence kinetic energy and also affects the dissipation rate.

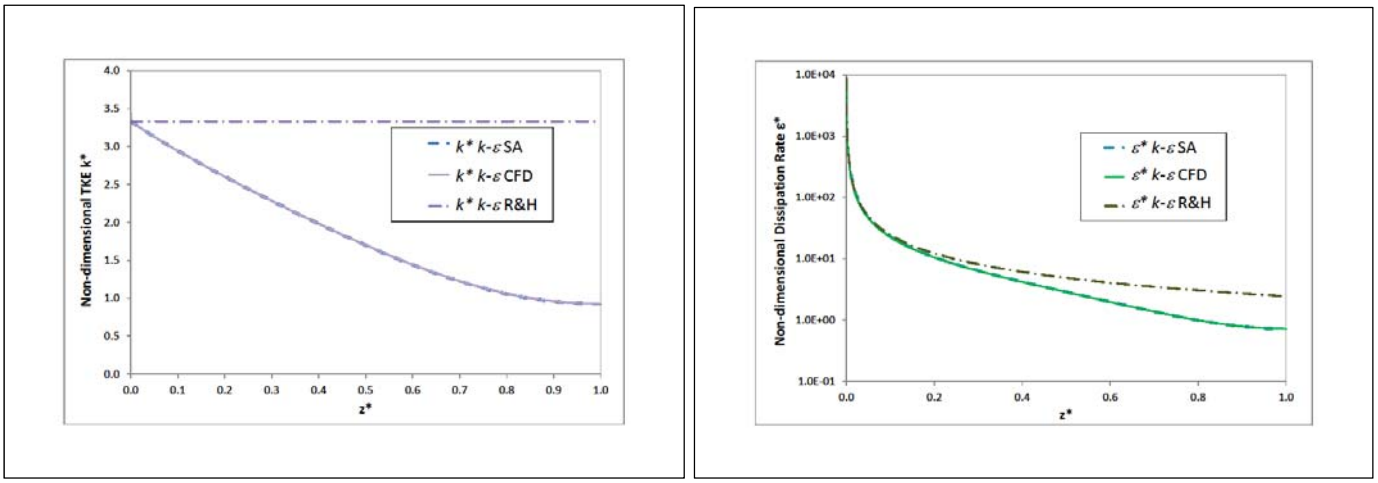

Fig. 7. (a) Turbulence kinetic energy and (b) dissipation profiles for shear (SA or CFD) and pressure (R&H) driven boundary layers.

With the k-ω model (Wilcox, 1993) the major difference from the standard k-ε model is that the second turbulence property solved is the specific dissipation

$$\omega = \frac{\varepsilon}{k\beta'} \tag{44}$$

The constant β' is equivalent to C_μ and also has a value of 0.09.

The conservation equations, equivalent to Eqs. (25) and (26), are:

$$\rho \frac{Dk}{Dt} = 0 = \mu_t \left(\frac{dU}{dz} \right)^2 - \beta' \rho k \omega + \frac{d}{dz} \left(\frac{\mu_t}{\sigma_{kW}} \frac{dk}{dz} \right) \tag{45}$$

$$\rho \frac{D\omega}{Dt} = 0 = \alpha \mu_t \left(\frac{dU}{dz} \right)^2 \frac{\omega}{k} - \beta \rho \omega^2 + \frac{d}{dz} \left(\frac{\mu_t}{\sigma_\omega} \frac{d\omega}{dz} \right) \tag{46}$$

with the supplementary equation

$$\mu_T = \rho \frac{k}{\omega} \tag{47}$$

and the model constants α=5/9, β=0.075, σ_{kW}=2 and σ_ω=2. These equations can be processed and solved in much the same way as the k-ε analysis. The polynomials for k^* and dU^*/dz^* take exactly the same form although the coefficients are slightly different as can be seen from Table 2. These can then be combined to provide a specific dissipation profile through

$$\omega = \frac{k}{u_\tau^2(1-z/H)}\frac{dU}{dz} = \frac{k(z)}{\kappa u_\tau z}\left(1+(1+U_1)(z/H)+(1+U_1+2U_2)(z/H)^2+(1+U_1+2U_2+3U_3)(z/H)^3\right) \quad (48)$$

Table 2: Polynomial coefficients for Eqs. (30) and (34).

	k_1	k_2	k_3	k_4	κ	U_1	U_2	U_3	U_4
k-ε SA	0.921	3.533	-1.926	0.805	0.4	0.528	0.385	-1.090	0.243
k-ε CFD	0.923	3.552	-1.994	0.852	0.415	0.784	0.055	-0.842	0.158
k-ω SA	0.810	4.046	-2.623	1.100	0.4	0.333	-0.666	0.465	-0.349
k-ω CFD	0.817	3.955	-2.385	0.946	0.407	0.368	-0.635	0.393	-0.319
SST CFD	1.056	2.814	-0.834	0.297	0.407	0.512	-0.772	0.072	-0.046

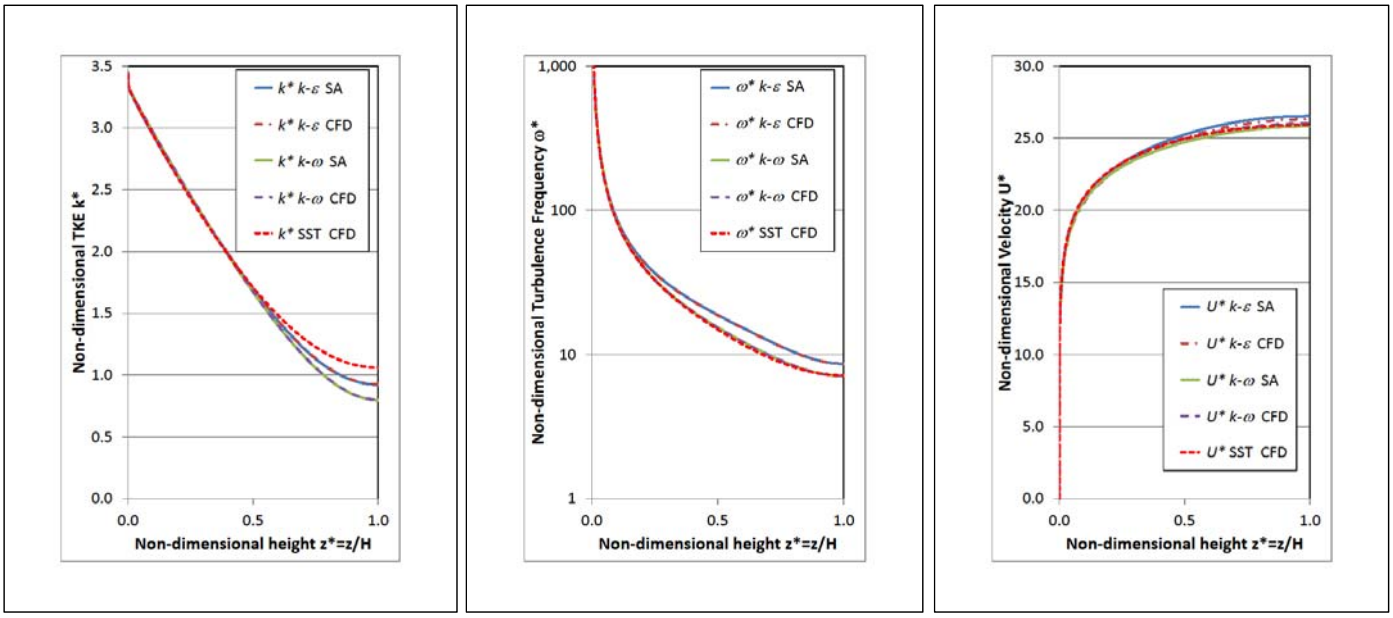

Fig. 8. Comparison of semi-analytic (SA) and CFD equilibrium profiles for 3 turbulence models. (a) Turbulence kinetic energy, (b) specific dissipation (where for the k-ε model the equivalent ω value has been calculated using Eq. (44)) and (c) velocity profiles.

The differences between the models is illustrated in Fig. 8, where in addition to the two semi-analytic solutions, CFD solutions, which will be discussed further in the following section, are provided for the 3 turbulence models. All of the profiles are very similar at low levels but diverge as the top of the domain is approached. This partially reflects the significant difference in the diffusion expressions where in Eq. (45) σ_{kW}=2 whereas with the k-ε model in Eq. (23) σ_k=1, which halves the diffusion of TKE. This difference is also clear in the values for k_1, which reflect the level of TKE at the top of the domain.

5. Numerical Modelling

In order to obtain comparable values from a CFD program, CFX version 14.0 has been used with cyclic boundary conditions to obtain equilibrium solutions. For the CFD solutions a domain height H=500m, a roughness length z_0 = 0.01 m and a pressure gradient of -0.00097 Pa/m was used in all cases. This has been integrated with the boundary condition U=0 at height z=z_0. The resulting data has been fitted in the same way as the semi-analytic solutions, except that κ was not forced to be 0.4, and the polynomial coefficients are given in Table 2. Close agreement is achieved between the semi-analytic (SA) and CFD results for both the k-ε and k-ω turbulence models. It should be noted that the polynomial coefficient are sensitive to small changes and that a small change in one coefficient can cause a dramatic change in another. It is therefore significant to note that in comparing the values

obtain from the semi-analytic and CFD methods there is generally closer agreement between the two solutions than between the turbulence models. For example both approaches have U_2 positive for the k-ε model whereas it is negative with both methods for the k-ω models. This changing of sign also occurs with U_3 and U_4. It therefore appears that both approaches have captured the same differences between the turbulence models. This is also clear in Fig. 9 where the two approaches provide almost identical results for each model, and noticeable differences between models.

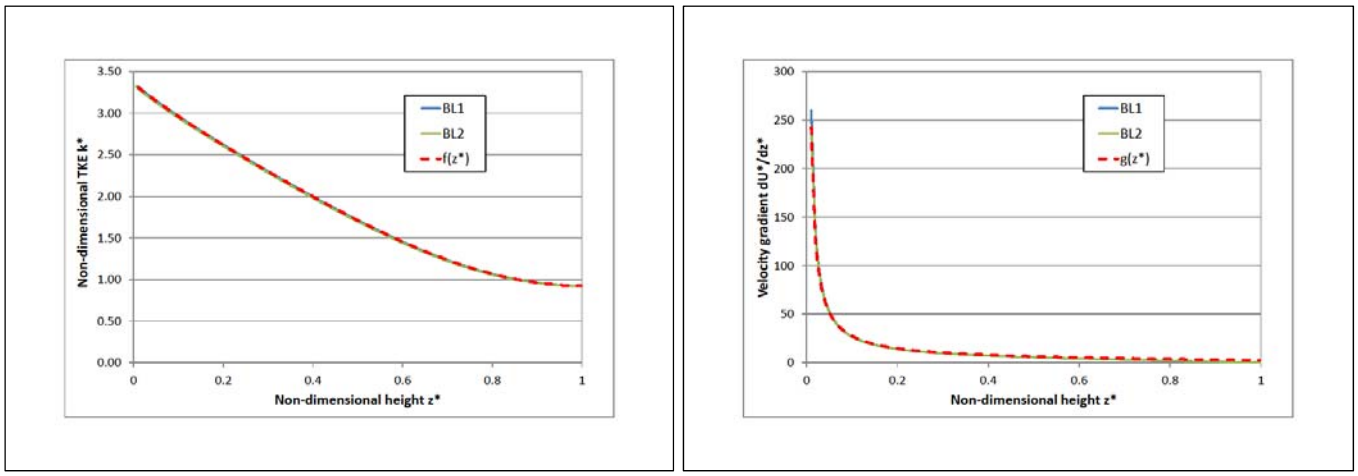

Fig. 9. Illustration of the universal nature of the functions (a) $f(z^*)$ and (b) $g(z^*)$.

During analysis of several CFD runs using the k-ε turbulence model it was recognised that if the TKE and velocity gradient results were plotted in a non-dimensional form, then they coalesced into in a single curve. This is illustrated in Fig. 8 for the two boundary layers whose parameters are given in Table 3. The two curves are almost indistinguishable. Also shown are the functions $f(z^*)$ and $g(z^*)$, as defined in Eqs. (31) and (36), which closely match both pairs of curves and hence may be considered to represent universal functions for any two-dimensional pressure driven boundary layer modelled using the k-ε turbulence model.

Table 3: Boundary layer parameters

	$U(10)$ (m/s)	z_0 (m)	H (m)	u_τ (m/s)
BL1	10	0.2	1000	1.05
BL2	5	0.1	100	0.45

To demonstrate the ability of these profiles to represent an equilibrium pressure driven boundary layer, these were prescribed at the inlet of flow through a long empty domain. The profiles at the outlet of the domain could then be compared with the inlet values, to see if the inlet values were actually in equilibrium, and also as a test of the ability of the CFD code solver to model such a flow. If the boundary conditions accurately describe the pressure driven flow, then there should be little difference between the values at the inlet and outlet of the domain.

The model problem used was the same as that given by Hargreaves and Wright (2007), and a schematic of the domain and the grid used is shown in Fig. 10. The inlet flow had a reference velocity of 10 m/s at a reference height of 6 m, with a ground roughness of $z_0 = 0.01$ m. The flow was modelled using CFX 14.0 using the standard k-ε model. Profiles of the velocity and the turbulence kinetic energy were extracted at the inlet and outlet of the domain and are plotted in Fig.s 11. Those labelled "Pressure …" use the inlet conditions derived in this paper for a pressure driven boundary layer. For comparison purposes, a calculation was also made using the Richards and Hoxey (1993) inlet profiles, which are intended for a shear driven boundary layer, but are deliberately misused here in conjunction with a free slip surface at the high-z boundary.

Fig. 11 shows that with the equilibrium profiles derived in this paper there is little difference between the inlet and outlet. There is a small change in TKE at low levels, which Richards and Norris (2011) show is caused by discretisation errors in the near wall region. In comparison the misuse of the Richards and Hoxey (1993) profiles results in significant changes between the inlet and outlet, most noticeably affecting the TKE profile since there is so much difference between the shear driven and pressure driven equilibrium situations. This change is also illustrated in Fig. 1. In contrast Fig. 12 shows the TKE development when the inlet is correctly matched to the pressure driven situation.

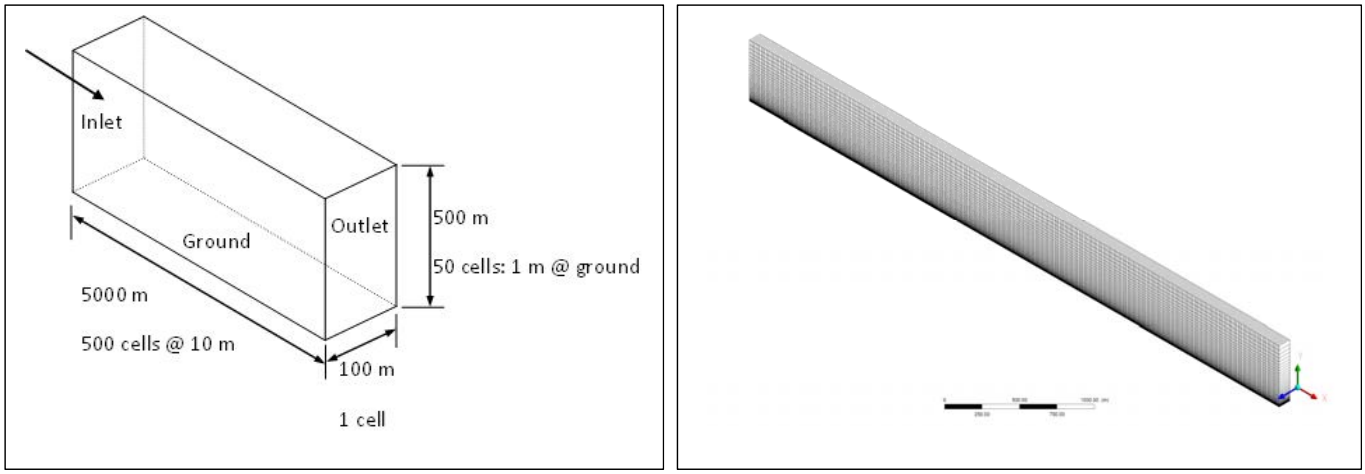

Fig. 10. (a) Schematic of the computational domain and (b) the corresponding grid.

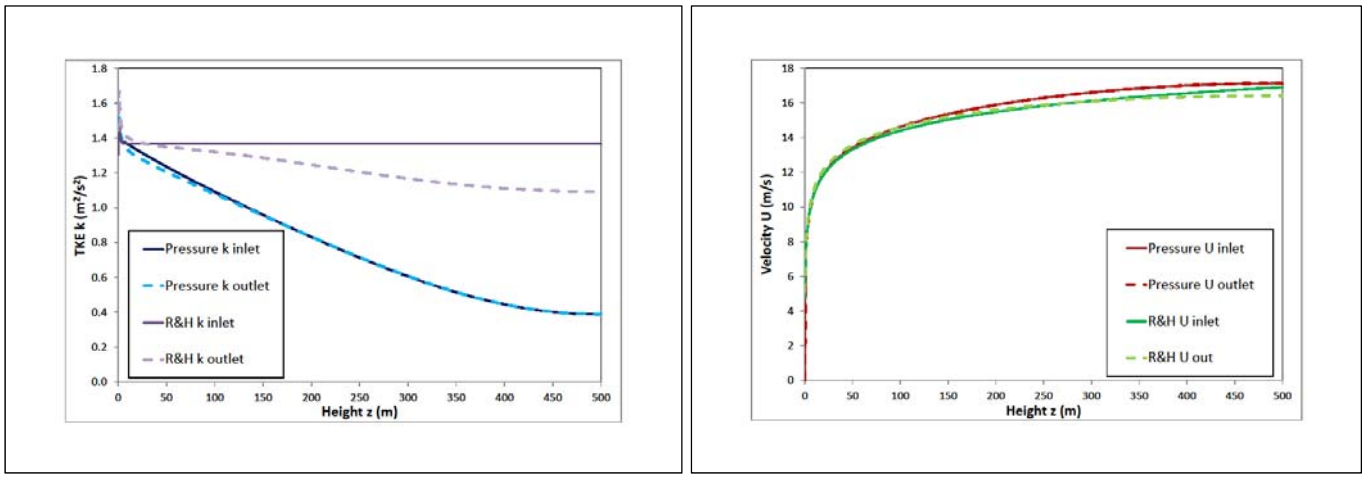

Fig. 11. Inlet and outlet (a) velocity and (b) TKE profiles using the equilibrium inlet profiles derived here in comparison with the misuse of the Richards and Hoxey inlet profiles.

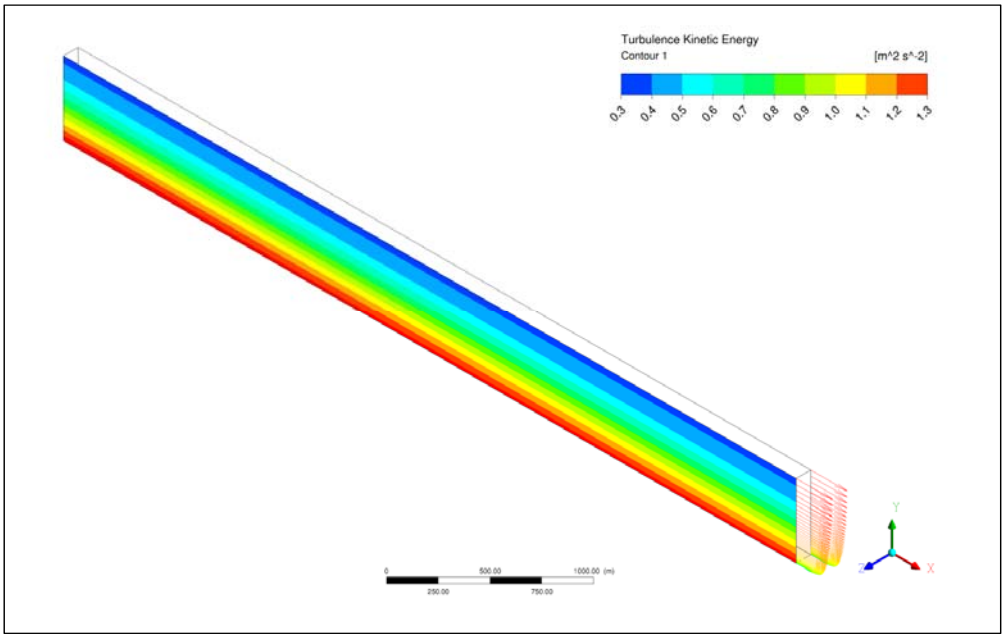

Fig. 12. Development of the turbulence kinetic energy in a pressure driven boundary layer with inlet conditions appropriate for this situation.

6. Appropriate Boundary Conditions for a Pressure Driven Boundary Layer

Based on the analysis presented in the previous sections it is recommended that if the atmospheric boundary layer is modelled as a pressure driven flow then the gradient height h should be estimated from

$$h = \frac{u_\tau}{6f} \tag{7}$$

and the domain height H set at half this height. The inlet velocity profile can then be calculated using Eq. (41).

$$U(z) = \frac{u_\tau}{\kappa}\left(\ln\left(\frac{z}{z_0}\right) + U_1\left(\frac{z}{H}\right) + U_2\left(\frac{z}{H}\right)^2 + U_3\left(\frac{z}{H}\right)^3 + U_4\left(\frac{z}{H}\right)^4\right) \tag{41}$$

Similarly the inlet turbulence profiles can be set by using Eqs. (42, 43 or 48) as appropriate. The suggested polynomial constants are given in Table 4. For the k-ε and Wilcox k-ω models these have been extracted directly from Table 2, where both solution techniques generated similar values. For the SST model the data has been reanalysed forcing von Karman's constant to κ=0.4 in order to bring it in line with the other two models. While this modifies the polynomial coefficients significantly the resulting velocity gradients only change by less than 4% across the entire boundary layer.

$$k(z) = u_\tau^2\left(k_1 + k_2\left(1-\frac{z}{H}\right)^2 + k_3\left(1-\frac{z}{H}\right)^4 + k_4\left(1-\frac{z}{H}\right)^6\right) \tag{42}$$

$$\varepsilon(z) = \frac{C_\mu k(z)^2}{\kappa u_\tau z}\left(1 + (1+U_1)(z/H) + (1+U_1+2U_2)(z/H)^2 + (1+U_1+2U_2+3U_3)(z/H)^3\right) \tag{43}$$

$$\omega(z) = \frac{k(z)}{\kappa u_\tau z}\left(1 + (1+U_1)(z/H) + (1+U_1+2U_2)(z/H)^2 + (1+U_1+2U_2+3U_3)(z/H)^3\right) \tag{48}$$

Table 4: Recommended Polynomial Coefficients

	k_1	k_2	k_3	k_4	κ	U_1	U_2	U_3	U_4
k-ε	0.921	3.533	-1.926	0.805	0.4	0.528	0.385	-1.090	0.243
k-ω	0.810	4.046	-2.623	1.100	0.4	0.333	-0.666	0.465	-0.349
SST	1.056	2.814	-0.834	0.297	0.4	0.280	-0.331	-0.334	0.096

While it is believed that these inlet boundary conditions can be used to generate an equilibrium pressure driven boundary layer, it is essential that they are combined with an appropriate rough wall treatment of the ground surface. In this regard it is important to note that many CFD codes use an equivalent sand grain roughness and that this is different from the wind engineering roughness length z_0 used in this paper. This aspect is discussed in detail by Blocken et al. (2007).

It is also noted that the above equations can be used to generate an equilibrium pressure driven boundary layer even if the domain height is less than half the gradient height. If the top of this shorter domain is a free-slip zero diffusion boundary then the shear stress gradient will be exaggerated and hence may affect results. If a shorter domain is necessary then a partial model is possible but a shear stress and associated turbulence diffusion sinks should be applied to the top of the domain. For example if the domain height is d and $d<h/2$ but the shear stress is assumed to decrease to zero a z=h/2, then the top of the domain has a shear stress

$$\tau(d) = \rho u_\tau^2(1-2d/h) \tag{49}$$

and the diffusion fluxes of k, ε or ω are

$$\mu_t(d)\left.\frac{dk}{dz}\right|_{z=d}, \quad \frac{\mu_t(d)}{\sigma_\varepsilon}\left.\frac{d\varepsilon}{dz}\right|_{z=d} \text{ or } \frac{\mu_t(d)}{\sigma_\omega}\left.\frac{d\omega}{dz}\right|_{z=d} \text{ respectively.} \tag{50}$$

Where the gradients can be determined by differentiating Eqs. (42), (43) or (48).

While only three turbulence models have been considered it is believed that these inlet profile would probably work reasonably well with many other turbulence models. The similarity of the profile in Fig. 7 suggests that the equilibrium profiles are more related to the shear stress variation than to the particular turbulence model and hence these results can be used as an approximation with any similar turbulence model.

7. Conclusions

CFD calculations of wind engineering flows often inappropriately use inlet boundary conditions derived for a shear driven flow but without the driving shear stress. Without this shear stress the flow being modelled is driven through the domain by a pressure gradient. By comparison with the Deaves and Harris model of the atmospheric boundary layer (ABL) it is demonstrated that a pressure driven boundary layer can be considered a reasonable model for the lower half of the ABL where the shear stress decreases approximately linearly with height. Boundary conditions have been derived for an equilibrium pressure driven flow using three common turbulence models. While no analytic solution has been found it is shown that the results can be fitted by simple polynomial equations. In non-dimensional form the profiles for the turbulence kinetic energy and the velocity gradients apply to all rough wall pressure driven equilibrium boundary layers. These profiles have been successfully applied to modelling flow through an empty computational domain such that the outlet conditions are almost the same as the inlet.

References

AS/NZS 1170.2:2011, Australia/New Zealand Standard, Structural design actions, Part 2: Wind actions, *Standards Australia Limited/Standards New Zealand*, 2011.

Bottema, M., Turbulence closure model "constants" and the problems of "inactive" atmospheric turbulence. *Journal of Wind Engineering and Industrial Aerodynamics*, 67&68, 1997, 897-908.

Blocken, B., Stathopoulos, T. & Carmeliet, J., CFD simulation of the atmospheric boundary layer: wall function problems. *Atmospheric Environment*, 41, 2007, 238-252.

Deaves D.M. & Harris R.I., A mathematical model of the structure of strong winds, CIRIA Report 76, Construction Industry Research and Information Association, London, 1978.

ESDU (1985), ESDU Data item 85020, Characteristics of atmospheric turbulence near the ground, Part II: single point data for strong winds (neutral atmosphere). Engineering Science Data Unit.

Franke, J., Recommendations of the COST action C14 on the use of CFD in predicting pedestrian wind environment. *Fourth International symposium on Computational Wind Engineering,* Yokohama, Japan, July 2006.

Hargreaves, D.M. & Wright, N.G., On the use of the k-ε model in commercial CFD software to model the neutral atmospheric boundary layer. *Journal of Wind Engineering and Industrial Aerodynamics*, 95, 2007, 355-369.

Launder, B.E. & Spalding, D.B., The numerical computation of turbulent flows. *Computer Methods in Applied Mechanics and Engineering*, 3, 1974, 269-289.

Norris, S.E., Richards, P.J., Mallinson, G.D., 2011, Improved finite volume discretisations of entropy generation and turbulence production, *Computers and Fluids*, 49, 302-311.

Panofsky, H.A. & Dutton J.A., *Atmospheric Turbulence*. Wiley-Interscience. 1984.

Richards, P.J. & Hoxey, R.P., Appropriate boundary conditions for computational wind engineering models using the k-ε turbulence model. *Journal of Wind Engineering and Industrial Aerodynamics,* 46 & 47, 1993, 145-153.

Richards, P.J., Hoxey, R.P., Connell, B.D., Lander, D.P., 2007, 'Wind tunnel modelling of the Silsoe Cube'. *Journal of Wind Engineering and Industrial Aerodynamics*, 95, 1384-1399.

Richards, P.J. & Norris, S.E., 2011, 'Appropriate boundary conditions for computational wind engineering models revisited', *Journal of Wind Engineering and Industrial Aerodynamics*, 99, 257-266.

Tominaga Y., Mochida A., Yoshie, R., Ktaoka H., Nozu T., Yoshikawa M. & Shirasawa T., AIJ guidelines for practical applications of CFD to pedestrian wind environment around buildings. *Journal of Wind Engineering and Industrial Aerodynamics*, 96, 2008, 1749-1761.

Yang, Y., Gu, M., Chen, S. & Jin X., New inflow boundary conditions for modelling the neutral equilibrium atmospheric boundary layer in computational wind engineering. *Journal of Wind Engineering and Industrial Aerodynamics*, 97, 2009, 88-95.